Analytical studies of PROTO-SPHERA equilibria

P. Buratti[1]†, B. Tirozzi[2], F. Alladio[1] and P. Micozzi[1]

[1]ENEA, Fusion and Nuclear Safety Department, C.R. Frascati, Via E. Fermi 45, 00044 Frascati (Roma) Italy

[2]Department of Physics, University La Sapienza of Rome, 00185 Roma, Italy

(Received xx; revised xx; accepted xx)

Analytical solutions of the Grad-Shafranov equilibrium equation in simply connected plasma configurations are reviewed and generalised. The Grad-Shafranov equation is linearised introducing assumptions on plasma current and pressure, which preserve regularity of solutions on the symmetry axis, as required for a simply-connected geometry. Particular solutions are found by separation of variables both in cylindrical coordinates and in spherical ones. Equilibria which model local or global features of PROTO-SPHERA plasmas are constructed by combining a few particular solutions.

1. Introduction

PROTO-SPHERA is a magnetic confinement experiment, aimed at sustaining axisymmetric plasmas in a simply connected magnetic configuration, i.e. without any solid structure placed between the plasma and the symmetry axis (Alladio *et al.* 2006; Lampasi *et al.* 2016). The toroidal magnetic field is generated by current flowing in a central pinch, the centerpost discharge, which is fed by electrodes; external conductors which return the centerpost current are the only residual components of a toroidal magnet. The main goal of the experiment is to form and confine fat plasma tori around the centerpost discharge, in a steady-state magnetic configuration, i.e. without relying on image currents in conducting structures.

The centerpost discharge is shaped by eight poloidal magnetic field coils in order to wet large-area annular electrodes. The centerpost plasma appears as a pinch with variable diameter for a length of about 1 m and**, after passing neck regions delimited by the bore of nearby shaping coils**, opens in the form of a mushroom in front of both annular electrodes, see figure 1(a). **The mushroom-shaped regions end with degenerate x-points (or triple nulls of the magnetic field) at the extremes along the axis.** Compression coils, with current of opposite sign to that of shaping coils, balance the expansion force of current-carrying plasma tori. The centerpost bright plasma has convex shape around the midplane when shaping coils only are activated. The bright region becomes concave as compression coils are activated, and a surrounding toroidal structure with different luminosity appears, see figure 1(b).

The experiment is presently operated with a reduced-current version of the compression coils, in order to assess the capability of producing fat tori around 10 kA centerpost discharges. The target configuration, with up to 70 kA centerpost current and up to 300 kA toroidal plasma current, will become available after upgrading the compression coils as well as the power supplies.

Magnetic field maps can be obtained from numerical equilibrium calculations that

† Email address for correspondence: paolo.buratti@enea.it

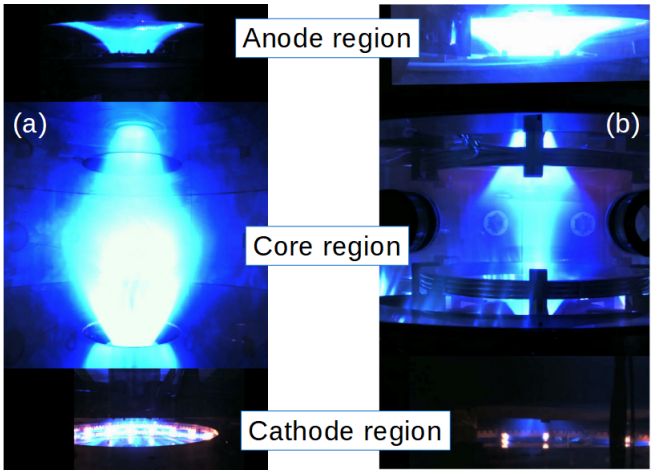

FIGURE 1. Visible light images of PROTO-SPHERA plasmas in Argon, as reconstructed from three cameras, one for the anodic region (top), one for the core region (middle) and one for the cathode (bottom). View at the transitions between different regions is impeded by poloidal field coils. (a) Plasma configuration obtained with shaping coils only. The centerpost is convex in the core region and no torus is present; **the mushroom-shaped region in front of the anode is uniform, while the cathodic one is filamented in correspondence with discrete electron emitters, which are visible as brilliant spots.** (b) Configuration with energized compression coils: the bright centerpost profile becomes concave, and a toroidal structure with different luminosity appears. Vision is further impeded in this setting by supporting structures of the compression coils.

include the actual shape of poloidal field coils; still analytical models are desirable in order to provide a simple geometric basis for advanced studies on **self-organisation of the configuration, in particular on how can toroidal current be sustained by** magnetic reconnection **in the absence of any applied toroidal electric field**.

Analytical equilibrium models developed to reproduce at least locally the different observed PROTO-SPHERA topologies are described in this work. Equilibrium equations for simply connected axisymmetric equilibria are introduced in section 2. Solutions obtained by variable separation in cylindrical coordinates and models based on such solutions are presented in sections 3 and 4 respectively. Solutions in spherical coordinates are obtained and and a model employing both cylindrical and spherical solutions is shown in section 5. Conclusions are given in section 6

2. Equilibrium in simply connected axisymmetric plasmas

Some well known results will be reviewed in this section, in order to provide a basis to discuss constraints on analytic solutions which arise in simply connected configurations .

2.1. *Axisymmetric fields*

Axial symmetry implies the gradient operator along the azimuthal versor $\mathbf{e}_\phi$ is null, $\mathbf{e}_\phi \cdot \boldsymbol{\nabla} = 0$, where ϕ is the azimutal (or toroidal) angle. All quantities (excepting ϕ) are constant on circles centered on the axis and lying on planes perpendicular to the axis. Poloidal magnetic flux (ψ) and poloidal current (I) linked by these circles are used to express the magnetic field in terms of scalar quantities and of $\boldsymbol{\nabla}\phi = \mathbf{e}_\phi/R$, R being distance from magnetic axis,

$$\mathbf{B} = \frac{1}{2\pi}\boldsymbol{\nabla}\psi \times \boldsymbol{\nabla}\phi + \frac{\mu_0 I}{2\pi}\boldsymbol{\nabla}\phi \equiv \mathbf{B}_{pol} + \mathbf{B}_{tor}. \tag{2.1}$$

The poloidal current I is entirely carried by the plasma in the simply-connected case, whereas it includes current carried by toroidal magnet coils in the tokamak case.

The poloidal field component ($\mathbf{B}_{pol}$) lies on poloidal cross sections (in-plane with the symmetry axis) while the toroidal one ($\mathbf{B}_{tor}$) lies on planes perpendicular to the symmetry axis. Magnetic field lines lie on constant-ψ surfaces (magnetic surfaces or flux surfaces).

The current density reads

$$\mathbf{j} = \frac{1}{2\pi}\boldsymbol{\nabla} I \times \boldsymbol{\nabla}\phi - \frac{R^2}{2\pi\mu_0}\boldsymbol{\nabla}\cdot\left(\frac{1}{R^2}\boldsymbol{\nabla}\psi\right)\boldsymbol{\nabla}\phi \equiv \mathbf{j}_{pol} + \mathbf{j}_{tor} \tag{2.2}$$

Magnetic flux ψ and current I are called poloidal flux and poloidal current respectively, for having contributions from poloidal components only. Poloidal flux is related to the azimuthal component of vector potential, $\psi = 2\pi R A_\phi$. In some textbooks the same symbol is used for poloidal flux divided by 2π.

The electromagnetic force density reads

$$\mathbf{j}\times\mathbf{B} = -\frac{1}{4\pi^2\mu_0}\boldsymbol{\nabla}\cdot\left(\frac{1}{R^2}\boldsymbol{\nabla}\psi\right)\boldsymbol{\nabla}\psi - \frac{\mu_0 I}{4\pi^2 R^2}\boldsymbol{\nabla} I \tag{2.3}$$

$\mathbf{B}\cdot\mathbf{j}\times\mathbf{B} = 0$ implies $\boldsymbol{\nabla} I \times \boldsymbol{\nabla}\psi = 0$; it follows $I = I(\psi)$, i.e. poloidal current is a flux function, constant on flux surfaces. Derivatives of flux functions will be indicated by a prime in the following,

$$I' \equiv \frac{\mathrm{d}I}{\mathrm{d}\psi} \tag{2.4}$$

The gradient of poloidal current is

$$\boldsymbol{\nabla} I = I'\ \boldsymbol{\nabla}\psi \tag{2.5}$$

2.2. *The Grad-Shafranov equation*

If inertial forces are negligible, the balance between electromagnetic force density and pressure gradient,

$$\mathbf{j}\times\mathbf{B} = \boldsymbol{\nabla} p \tag{2.6}$$

implies $\mathbf{B}\cdot\boldsymbol{\nabla} p = 0$. Since, by axisymmetry, $\boldsymbol{\nabla}\phi\cdot\boldsymbol{\nabla} p = 0$, it follows $\boldsymbol{\nabla} p \times \boldsymbol{\nabla}\psi = 0$ and then pressure is a flux function, $p = p(\psi)$. In this condition, force balance can be expressed by the Grad-Shafranov (GS) equation

$$\frac{1}{4\pi^2\mu_0}\boldsymbol{\nabla}\cdot\left(\frac{1}{R^2}\boldsymbol{\nabla}\psi\right) + \frac{\mu_0 I}{4\pi^2 R^2} I' = -p' \tag{2.7}$$

where R is distance from the symmetry axis and primes denote derivatives with respect to ψ.

If inertia is not negligible, e.g. if there is substantial plasma rotation, pressure is not a flux function and a more general treatment (outside the scope of this work) is required.

2.3. *Linear models*

Plasma equilibrium configurations are usually calculated via numerical solutions of the GS equation, assuming parametric functional forms of $I(\psi)$ and $p(\psi)$ and determining parameters by iterative numerical schemes.

Exact analytical solutions solutions of the GS equation have been used to benchmark numerical equilibrium codes, as well as to provide initial conditions for stability analysis in tokamaks. Families of exact tokamak equilibria have been found by assuming particular forms of the $I(\psi)$ and $p(\psi)$ functions for which the GS equation becomes linear (Solov'ev 1968; Guazzotto & Freidberg 2007; Xu & Fitzpatrick 2019).

Analytical equilibrium models are also desirable in the context of PROTO-SPHERA activities, in particular to provide a simple geometric basis for advanced studies on magnetic reconnection as well as on plasma transport. Analytical modelling of equilibrium in simply connected plasma configurations like PROTO-SPHERA entails the constraint of regularity at the symmetry axis ($R = 0$). For example, the choice of constant $I\,I'$, which gives compact and flexible solutions in the toroidal case (Solov'ev 1968; Xu & Fitzpatrick 2019), **is not acceptable as it** results in singular current density at $R = 0$. The reason is that, **being surface integrals of non-singular vector fields,** both ψ and I should increase like R^2 near the axis, whereas constant $I\,I'$ implies $I \propto R$, i.e. singular poloidal current density.

The assumption on poloidal current adopted in this work is $I \propto \psi$, **i.e. constant I', which linearizes the GS equation while avoiding** the singularity at the symmetry axis. The constant of proportionality is expressed in terms of the poloidal current parameter,

$$\mu = \mu_0\, I'. \tag{2.8}$$

The assumption on $p(\psi)$ is the same as in (Solov'ev 1968),

$$4\pi^2 \mu_0\, p' = \alpha, \tag{2.9}$$

where α is a constant. In the force-feree case ($\alpha = 0$), the poloidal current parameter μ is equivalent to the Taylor relaxation parameter (Taylor & Turner 1989), whereas in general the poloidal current density only is relaxed:

$$\mu_0 \mathbf{j}_{pol} = \mu \mathbf{B}_{pol}; \qquad \mu_0 j_{tor} = \mu B_{tor} + \frac{\alpha R}{2\pi}. \tag{2.10}$$

With assumptions (2.8) and (2.9), the GS equation becomes

$$R^2\ \boldsymbol{\nabla} \cdot \left(\frac{1}{R^2} \boldsymbol{\nabla} \psi \right) + \mu^2 \psi = -\alpha R^2. \tag{2.11}$$

Equilibrium models presented in the following sections involve combinations of solutions of the force-free equation

$$R^2\ \boldsymbol{\nabla} \cdot \left(\frac{1}{R^2} \boldsymbol{\nabla} \psi \right) + \mu^2 \psi = 0 \tag{2.12}$$

with the particular solution of (2.11)

$$\psi_p = -\frac{\alpha}{\mu^2} R^2, \tag{2.13}$$

which, according to (2.1), corresponds to a uniform magnetic field parallel to the symmetry axis.

Equation (2.12) is separable both in cylindrical coordinates and in spherical ones. Solutions are developed in the following for each case, and simple models obtained by combining a few terms of the general solutions are discussed.

3. Equilibrium solutions in cylindrical coordinates

Equation (2.12) in (R, ϕ, Z) cylindrical coordinates becomes

$$R\frac{\partial}{\partial R}\left(\frac{1}{R}\frac{\partial \psi}{\partial R}\right) + \frac{\partial^2 \psi}{\partial Z^2} + \mu^2 \psi = 0. \tag{3.1}$$

Magnetic field components are

$$B_R = -\frac{1}{2\pi R}\frac{\partial \psi}{\partial Z}, \tag{3.2a}$$

$$B_Z = \frac{1}{2\pi R}\frac{\partial \psi}{\partial R}, \tag{3.2b}$$

$$B_\phi = \frac{1}{2\pi R}\mu\psi. \tag{3.2c}$$

Separation of variables in the form $\psi_n(R, Z) = R f_n(R) g_n(Z)$, where the subscript index **labels individual solutions as determined by a separation paramenter** k_n, gives standard equations for g_n and f_n,

$$\frac{\mathrm{d}^2 g_n}{\mathrm{d}Z^2} + k_n^2 g_n = 0, \tag{3.3}$$

$$R^2\frac{\mathrm{d}^2 f_n}{\mathrm{d}R^2} + R\frac{\mathrm{d}f_n}{\mathrm{d}R} + \left(\left(\mu^2 - k_n^2\right)R^2 - 1\right) f_n = 0. \tag{3.4}$$

Real solutions of (3.3) are

$$g_n(Z) = \cos(k_n(Z - Z_n)), \tag{3.5}$$

showing that the k_n parameter introduced by separation is an inverse length scale in the axial direction.

Equation (3.4) is a Bessel equation for $\mu \neq k_n$ and it reduces to an Euler equation for $\mu = k_n$; its real, non-singular solutions are

$$f_n(R) = \mathrm{I}_1(\sqrt{|\mu^2 - k_n^2|}\, R)/\sqrt{|\mu^2 - k_n^2|} \quad \text{as } \mu < k_n, \tag{3.6a}$$

$$f_n(R) = R/2 \quad \text{as } \mu = k_n, \tag{3.6b}$$

$$f_n(R) = \mathrm{J}_1(\sqrt{\mu^2 - k_n^2}\, R)/\sqrt{\mu^2 - k_n^2} \quad \text{as } \mu > k_n, \tag{3.6c}$$

where J_1 and I_1 denote Bessel functions of the first kind and modified Bessel functions of the first kind respectively, and denominators have been chosen to have continuity as μ/k_n changes. Solutions similar to (3.6c) were considered in (Jensen & Chu 1981; Furth *et al.* 1957).

Model equilibria can be constructed superposing individual solutions from (3.5), (3.6) and the particular solution (2.13),

$$\psi(R, Z) = \sum_{n=0} b_n R f_n(R) \cos(k_n(Z - Z_n)) - \frac{\alpha}{\mu^2}R^2. \tag{3.7}$$

The sum in (3.7) reduces to a Fourier series in Z if $k_n = nk_1$, i.e. if the separation parameters are multiples of a fundamental scale. **A Fourier decomposition could then be used to obtain b_n coefficients and Z_n shifts for an assigned $Z-$profile of ψ at constant R. A complementary approach is followed in this work, the characteristics of up-down symmetric configurations ($Z_n = 0$) obtainable with a few terms of the sum are studied for different values of the b_n coefficients.**

4. Equilibrium models in cylindrical coordinates

The topological features of equilibria which can be constructed from (3.7) can be illustrated considering just two terms of the sum. A periodic structure is obtained in this way, with a single period representing the core region as defined in figure 1. The mushroom-shaped regions are outside the scope of the present analysis. **The force-free case ($\alpha = 0$) is considered at first; the pressure term is then reintroduced at the end of this section.**

The model with two terms is an extension of the bumpy pinch analytical model suggested by Taylor (Jensen & Chu 1981). The first term must have $k_0 = 0$, as required to have open field lines around the $R = 0$ axis. The second term must have $k_1 = \pi/L$, where L is the half length of the core region. The origin of the Z coordinate is chosen to have $Z_1 = 0$. Introducing the normalisation $\rho = k_1 R$, $\zeta = k_1 Z$, $\hat{\mu} = \mu/k_1$, and $\gamma_1 = b_1/b_0$, the model flux takes a form which depends on $\hat{\mu}$ and γ_1 only,

$$\frac{k_1^2}{b_0}\psi(\rho,\zeta) = \frac{\rho}{\hat{\mu}}\mathrm{J}_1(\hat{\mu}\rho) + \gamma_1\rho\hat{f}_1(\rho)\cos(\zeta), \tag{4.1}$$

where

$$\hat{f}_1(\rho) = \mathrm{I}_1(\sqrt{|\hat{\mu}^2-1|}\,\rho)/\sqrt{|\hat{\mu}^2-1|} \qquad \text{as } \hat{\mu} < 1, \tag{4.2a}$$

$$\hat{f}_1(\rho) = \rho/2 \qquad \text{as } \hat{\mu} = 1, \tag{4.2b}$$

$$\hat{f}_1(\rho) = \mathrm{J}_1(\sqrt{\hat{\mu}^2-1}\,\rho)/\sqrt{\hat{\mu}^2-1} \qquad \text{as } \hat{\mu} > 1, \tag{4.2c}$$

The topology of flux surfaces depends on the sign of γ_1. Negative values correspond to magnetic configurations produced in the experiment by shaping coils only. Positive values correspond to configurations produced when compression coils are activated.

If $\gamma_1 < 0$, there is a single x-point at the equatorial plane, see figure 2; all flux surfaces are open in this case and their shape is bulgy around the equatorial plane, consistent with the pinch-only experimental case shown in figure 1(a). The x-point location shifts inwards with increasing $\hat{\mu}$ as well as with increasing $|\gamma_1|$, as shown in figure 2.

If on the contrary $\gamma_1 > 0$, an equatorial o-point surrounded by closed flux surfaces (i.e. a magnetic axis) appears, with two x-points at $\zeta = \pm\pi$, as shown in figure 3(a). Open flux contours appear squeezed around the equatorial plane, consistent with the experimental case shown in figure 1(b).

This kind of configuration only exists if $\hat{\mu}$ is above a critical value, otherwise the outer branch of the separatrix breaks out, as shown in figure 3(b). The critical value increases with γ_1, from 0.6 at $\gamma_1 = 0.01$ to 0.9 at $\gamma_1 = 0.1$ to 1.2 at $\gamma_1 = 0.5$. This indicates that the higher the applied compression field the more plasma current is required to form the configuration. The possibility of a localised equilibrium crisis in response to small variations of plasma current could play a role in plasma dynamics.

As $\hat{\mu}$ increases above the critical value, the distance between the two branches of the separatrix decreases, i.e. elongation increases. The x-points shift inwards and the o-point slightly shifts outwards (i.e. triangularity increases) with increasing γ_1 at constant $\hat{\mu}$, see figure 4.

When including **a dimensionless form of the last term in (3.7), which represents** finite plasma pressure, the model **normalised flux** becomes

$$\frac{k_1^2}{b_0}\psi(\rho,\zeta) = \frac{\rho}{\hat{\mu}}\mathrm{J}_1(\hat{\mu}\rho) + \gamma_1\rho\hat{f}_1(\rho)\cos(\zeta) - \frac{1}{2\pi}\beta\rho^2, \tag{4.3}$$

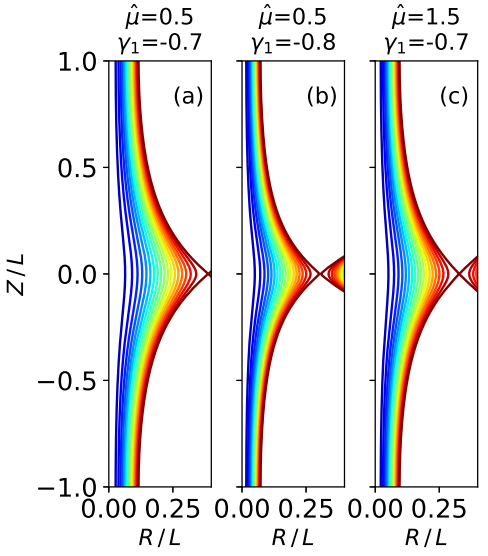

FIGURE 2. Poloidal flux contour plots in a constant-ϕ (poloidal) cross section for $\gamma_1 < 0$. (a) Reference case with moderate values of both $\hat{\mu}$ and $|\gamma_1|$ parameters. (b) Effect of larger $|\gamma_1|$. (c) Effect of larger $\hat{\mu}$. Coordinates are normalised to half axial length, $R/L = \rho/\pi$ and $Z/L = \zeta/\pi$.

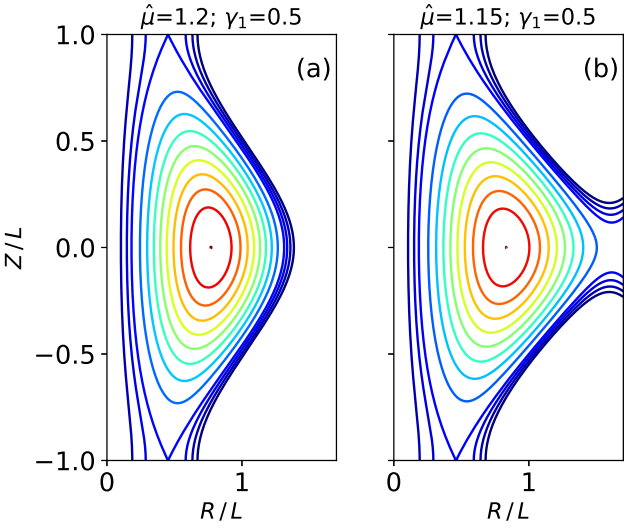

FIGURE 3. Poloidal flux contour plots in a constant-ϕ (poloidal) cross section for $\gamma_1 > 0$. (a) Configuration with $\hat{\mu}$ above the critical value: Both branches of the separatrix between open and closed flux surfaces are continuous. (b) Configuration with $\hat{\mu}$ slightly below the critical value: The outer separatrix branch breaks out. Coordinates are normalised to half axial length, $R/L = \rho/\pi$ and $Z/L = \zeta/\pi$.

where the β parameter, defined as

$$\beta \equiv \frac{2\pi\alpha}{b_0\mu^2}, \tag{4.4}$$

nearly (to within 20%) equals the plasma beta $2\mu_0 p/B^2$ at the magnetic axis. Triangu-

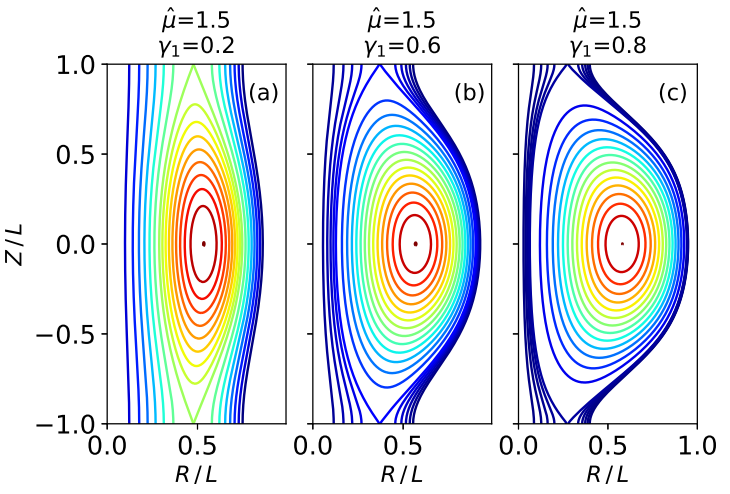

FIGURE 4. Variation of plasma shape with increasing γ_1 at fixed $\hat{\mu} = 1.5$ (well above the critical value). Coordinates are normalised to half axial length, $R/L = \rho/\pi$ and $Z/L = \zeta/\pi$.

larity increases with increasing β, as shown in figure 5, **consistent with the fact that inclusion of finite plasma pressure adds a uniform B_Z contribution, which tends to shift x-points towards the axis.**

The condition of open field lines existence gives restrictions on model parameters. Open field lines (which have to occupy a finite bore corresponding to the centerpost discharge) disappear as a zero appears in the axial profile of B_Z. From (3.2b), using the derivation rules $(x\mathrm{J}_1(x))' = x\mathrm{J}_0$ and similar for I_1,

$$B_Z(0,\zeta) = \frac{b_0}{2\pi}\left(1 + \gamma_1\cos(\zeta) - \frac{\beta}{\pi}\right). \tag{4.5}$$

The condition $\min(B_Z) > 0$ gives both the equilibrium beta limit $\beta < \pi(1 - |\gamma_1|)$ and the shaping parameter limit in the force-free limit, $|\gamma_1| < 1$.

5. Equilibrium model in mixed coordinates

5.1. *Solutions in spherical coordinates*

Equation (2.12) in (r, θ, ϕ) spherical coordinates, where $r = (R^2 + Z^2)^{1/2}$ and $\tan\theta = R/Z$, takes the form

$$\frac{\partial^2\psi}{\partial r^2} + \frac{\sin\theta}{r^2}\frac{\partial}{\partial\theta}\left(\frac{1}{\sin\theta}\frac{\partial\psi}{\partial\theta}\right) + \mu^2\psi = 0. \tag{5.1}$$

Separation of variables $\psi_n(r,\theta) = \psi_{n1}(r)\,\psi_{n2}(x)$, with $x = \cos\theta$, gives

$$\frac{r^2}{\psi_{n1}}\frac{\mathrm{d}^2\psi_{n1}}{\mathrm{d}r^2} + r^2\mu^2 = -\frac{1-x^2}{\psi_{n2}}\frac{\mathrm{d}^2\psi_{n2}}{\mathrm{d}x^2} = n(n+1), \tag{5.2}$$

where n is a separation parameter. With the change of variable $\psi_{n2} = (1-x^2)^{1/2}p(x)$, the angular part of (5.2) becomes a general Lagrange equation of degree n and order 1, with solution $p(x) = P_n^1(x)$. For integer n the angular dependence becomes a combination of

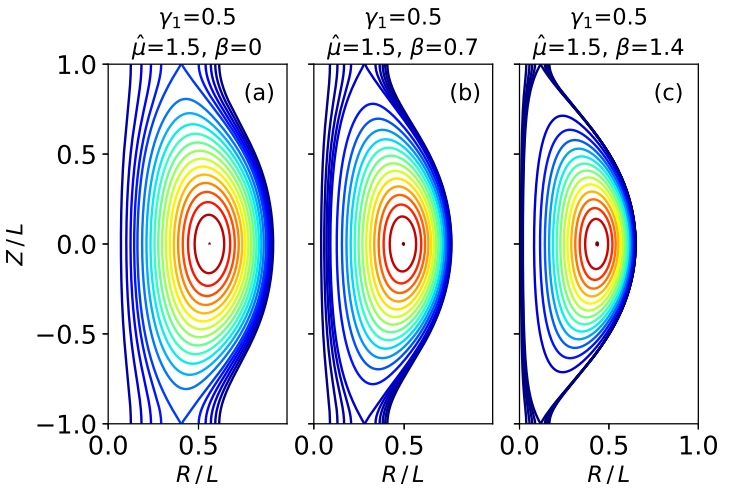

FIGURE 5. Poloidal flux contour plots in a constant-ϕ (poloidal) cross section for increasing β at constant values of both $\hat{\mu}$ and γ_1; (a) force-free case, (b) intermediate β, (c) β close to the equilibrium limit. Coordinates are normalised to half axial length, $R/L = \rho/\pi$ and $Z/L = \zeta/\pi$.

Legendre polynomials,

$$\psi_{n2}(x) = n\mathrm{P}_{n-1}(x) - nx\mathrm{P}_n(x). \tag{5.3}$$

The equation for the radial dependence transforms into a Bessel equation with the change of variable $\psi_{n1}(r) = \mu r q(r)$. The solution for integer n is a spherical Bessel function, $q(r) = \mathrm{j}_n(\mu r)$, so that the generic solution for integer n is

$$\psi_n(r,\theta) = \mu r \mathrm{j}_n(\mu r)\,(n\mathrm{P}_{n-1}(\cos\theta) - n\cos\theta \mathrm{P}_n(\cos\theta)). \tag{5.4}$$

Equivalent solutions have been obtained in (Chandrasekhar 1956; Chandrasekhar & Kendall 1957). The $n = 1$ solution will be used in the next subsection.

5.2. *The Chandrasekhar-Kendall-Furth model*

The $n = 1$ spherical solution, indicated as ψ_{spher} in the following, can be modified to reproduce some global aspects of PROTO-SPHERA equilibria (Rogier *et al.* 2003), in particular the presence of a core plasma region and of two mushroom-shaped expansions in front of the electrodes, connected to the core region by relatively narrow sections. Another relevant feature is the presence of triple nulls of the magnetic field at the extremes along the axis of the mushroom-shaped parts.

Contour plots of the $n = 1$ spherical solution,

$$\psi_{spher} = \mu r \mathrm{j}_1(\mu r)\sin^2\theta, \tag{5.5}$$

where Legendre polynomials have been replaced by their explicit expressions, are shown in figure 6. Three regions with closed flux surfaces, separated by zeros of $\mathrm{j}_1(\mu r)$ at $\mu r_1 \approx 4.4934$, $\mu r_2 \approx 7.7253$, and $\mu r_3 \approx 10.9041$, can be seen in figure 6, where boundary lines appear as quarters of circle intersecting the Z-axis. Points of intersection with the Z-axis are triple magnetic nulls. The inner region (with positive flux, ending at $r = r_1$) can be modified to reproduce the core plasma (as defined in figure 1), provided that some of its surfaces

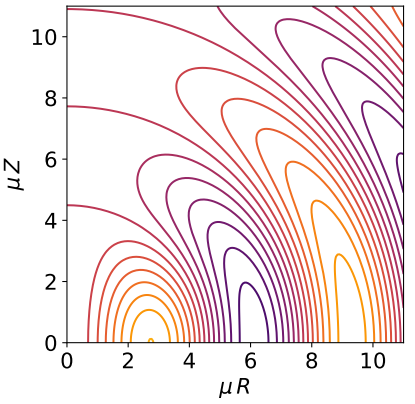

FIGURE 6. Constant poloidal flux contours for the $n = 1$ solution obtained from separation of variables in spherical coordinates. $R = r\sin\theta$ and $Z = r\cos\theta$ coordinates are normalised by the length scale associated to the poloidal current parameter. Hot colors correspond to positive values

become connected with ones of the outer region. The outer region ($r_2 < r < r_3$, again with positive flux) can then be transformed into the expanded centerpost in front of the electrodes (the configuration is up-down symmetric, the upper part only is shown in figure 6). The negative-flux region in the middle ($r_1 < r < r_2$) forms the neck regions lying between core plasma and expanded centerpost regions. This topological change can be accomplished by superposing a different equilibrium solution to (5.5), in order to introduce a bridge with positive flux across the negative-flux region. An additional request is to preserve the presence of a triple magnetic null at the end of the configuration along the axis. Both requests can be fulfilled by superposing a solution having the form presented in section 3,

$$\psi_{cyl}(R, Z) = (\mu^2 - k^2)^{1/2} R\, \mathrm{J}_1((\mu^2 - k^2)^{1/2} R)\, \cos(kZ), \tag{5.6}$$

with

$$k = \frac{\pi}{2x_3}\mu, \tag{5.7}$$

such that the triple null of ψ_{cyl} coincides with the third null of ψ_{spher}. A constant factor has been introduced in (5.6) for consistency with (Rogier *et al.* 2003). The n subscript has been removed in (5.6) since a single k is involved, and the $\mu > k$ form of (3.6) has been used, consistent with (5.7).

The superposition of (5.5) and (5.6),

$$\psi_{CKF} = \psi_{spher} + \gamma\, \psi_{cyl}, \tag{5.8}$$

where γ is the superposition coefficient, has been dubbed (Rogier *et al.* 2003) Chandrasekhar-Kendall-Furth force-free field (CKF), for being based on particular equilibrium solutions from (Chandrasekhar & Kendall 1957; Furth *et al.* 1957).

The shape of CKF configurations does not depend on the poloidal current parameter, in fact μ variations are equivalent to rescaling both R and Z with the same factor. The dimensional half-length of the configuration, defined as the distance between the origin and each of the triple null points, is $L = x_3/\mu$.

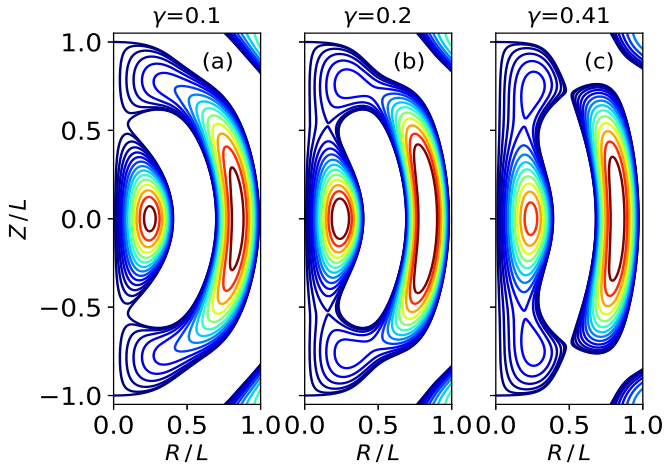

FIGURE 7. Constant flux contours of CKF models with superposition coefficient (a) $\gamma = 0.1$, (b) $\gamma = 0.2$ and (c) $\gamma = 0.41$. Coordinates are normalised to half axial length. Regions with negative flux appear as white areas, as negative contours levels are not shown.

CKF configurations change dramatically as the γ superposition coefficient increases. A representative sequence is shown in figure 7. For $\gamma = 0.1$, see figure 7(a), some contours that surround both positive-flux regions appear, and the tips of these regions get in contact at two x-points, while the negative-flux region, which is represented by a white area, becomes detached from the Z-axis. For $\gamma = 0.2$, contours lying between the separatrix and the Z-axis become visible, see figure 7(b). Their shape resembles visible camera images of the centerpost discharge for the rapid turning in proximity of triple null points. Meanwhile, the outer positive region tends to break, as shown by the appearance of some droplet-shaped contours. For $\gamma > 0.402$ the outer positive region breaks apart, resulting in a configuration with two closed secondary tori on top and on bottom of the main torus, see figure 7(c). This kind of configuration was used in (Rogier *et al.* 2003) as a basis for ideal MHD stability studies, as well as for conceptual studies on plasma propulsion. Secondari tori completely merge with the main torus as γ increases above 0.69.

Equilibrium models based on the CKF configuration complement the ones presented in section 3, for being less flexible but more global.

6. Concluding remarks

Analytical models of PROTO-SPHERA equilibria have been developed in order to provide a simple geometric basis for studies on self-organisation of the configuration.

The Grad-Shafranov equilibrium equation has been linearised adopting prescriptions the fulfill regularity of solutions in a domain that includes the symmetry axis, as required to model PROTO-SPHERA simply connected configurations.

Particular solutions obtained with separation of variables in cylindrical coordinates have been used to construct a simple equilibrium model, which can locally (in the plasma core region) reproduce different plasma topologies which can be observed in the

experiment. This model shows a criticality of equilibrium topology, due to break out at low plasma current of the outer branch of the separatrix between closed and open flux surfaces, an effect that could play a role in plasma dynamical processes.

Other solutions have been obtained with separation of variables in spherical coordinates. A model that allows reproducing the presence of three different plasma regions (anodic, core and cathodic) in the actual PROTO-SPHERA configuration has been implemented by combining a spherical solution with a cylindrical one.

REFERENCES

Alladio, F., Costa, P., Mancuso, A., Micozzi, P., Papastergiou, S. & Rogier, F. 2006 Design of the PROTO-SPHERA experiment and of its first step (MULTI-PINCH). *Nucl. Fusion* **46**, S613–S624.

Chandrasekhar, S. 1956 On force-free magnetic fields. *Proc. Nat. Acad. Sci.* **42**, 1.

Chandrasekhar, S. & Kendall, P. C. 1957 On force-free magnetic fields. *Astrophys. J.* **41**, 457.

Furth, H. P., Levine, M. A. & Wantek, R. W. 1957 Production and Use of High Transient Magnetic Fields. II. *Rev. Sci. Instr.* **28**, 949.

Guazzotto, L. & Freidberg, J. P. 2007 A family of analytic equilibrium solutions for the Grad–Shafranov equation. *Phys. Plasmas* **14**, 112508.

Jensen, T. H. & Chu, M. S. 1981 The bumpy Z-pinch. *J. Plasma Phys.* **25**, 459.

Lampasi, A. & others 2016 Progress of the Plasma Centerpost for the PROTO-SPHERA spherical tokamak. *Energies* **9**, 508.

Rogier, F., Bracco, G., Mancuso, A., Micozzi, P. & Alladio, F. 2003 Simply Connected High-β Magnetic Configurations. *AIP Conf. Proc.* **669**, 557.

Solov'ev, L. S. 1968 The theory of hydromagnetic stability of toroidal plasma configurations. *Sov. Phys.-JETP* **26**, 400.

Taylor, J. B. & Turner, M. F. 1989 Plasma current drive by helicity injection in relaxed states. *Nucl. Fusion* **29**, 219.

Xu, T. & Fitzpatrick, R. 2019 Vacuum solution for Solov'ev's equilibrium configuration in tokamaks. *Nucl. Fusion* **59**, 064002.